Supporting Information for

On the breakdown of Förster energy transfer theory due to solvent effects: Atomistic simulations unveil distance-dependent dielectric screening in calmodulin

Daniel Gonzalo,[1,2] Lorenzo Cupellini[3] and Carles Curutchet[1,2*]

[1]Departament de Farmàcia i Tecnologia Farmacèutica, i Fisicoquímica, Facultat de Farmàcia i Ciències de l'Alimentació, Universitat de Barcelona (UB), Barcelona, Spain

[2]Institut de Química Teòrica i Computacional (IQTCUB), Universitat de Barcelona (UB), Barcelona, Spain

[3]Dipartimento di Chimica e Chimica Industriale, Università di Pisa, 56126 Pisa, Italy

1. Methods

1.1 Förster resonance energy transfer theory

Förster theory is formulated in the weak coupling limit according to the golden rule expression,[1]

$$k_{FRET} = \frac{2\pi}{\hbar} V^2 J \tag{S1}$$

where V is the electronic coupling between D/A molecules, and J the spectral overlap factor obtained from the area-normalized donor emission and acceptor absorption spectra. Förster theory approximates the coupling assuming a point dipole approximation (PDA) and a simple screening factor s,

$$V \approx sV_{PDA} = \frac{1}{n^2} V_{PDA} = \frac{1}{n^2} \frac{\kappa \mu_D \mu_A}{R^3} \tag{S2}$$

where μ_D and μ_A are the D/A transition dipole moments, κ the dipole orientation factor, R the D/A center-to-center distance, and n the refractive index of the medium.

Alternatively, Förster rate can be formulated from purely spectroscopic data,

$$k_{FRET} = k_D \left(\frac{R_o}{R}\right)^6 = \frac{1}{\tau_D} \left(\frac{R_o}{R}\right)^6 \tag{S3}$$

where $k_D = 1/\tau_D$ indicates the decay rate of the excited D in the absence of A based on its lifetime τ_D, and R_o the critical quenching radius or Förster radius (in nm), which corresponds to the distance with 50% efficiency,

$$R_0^6 = \frac{9 \ln 10}{128 \pi^5 N_A} \frac{\kappa^2 \phi_D I}{n^4} \tag{S4}$$

where N_A is the Avogadro constant (in mol^{-1}), ϕ_D the fluorescence quantum yield, and I the spectral overlap (in M^{-1} cm^{-1} nm^4). Starting from this definition, the transfer efficiency can be expressed as

$$E_{FRET} = \frac{k_{FRET}}{k_D + k_{FRET}} = \frac{1}{1 + (R/R_0)^6} \tag{S5}$$

From the above expressions Eq. (S1)-(S3), one can derive the spectral overlap factor J from the experimental R_o value, tabulated for specific dye pairs assuming an isotropic orientation factor $\kappa^2 = 2/3$:

$$k_{FRET} = \frac{2\pi}{\hbar}\left(\frac{1}{n^2}\frac{\kappa\mu_D\mu_A}{R^3}\right)^2 J = \frac{1}{\tau_D}\left(\frac{R_o}{R}\right)^6 \quad \text{(S6)}$$

$$\frac{2\pi}{\hbar}J = \frac{3n^4R_0^6}{2\tau_D\mu_D^2\mu_A^2} \quad \text{(S7)}$$

Then, it is possible to compute the instantaneous transfer rate using different approximations for the coupling V computed at time t of an MD trajectory using the following expression, which combines Eq. (S1) and (S7):

$$k_{theo}(t) = V(t)^2\frac{3n^4R_0^6}{2\tau_D\mu_D^2\mu_A^2} \quad \text{(S8)}$$

If we adopt the PDA approximation, a simpler expression follows:

$$k_{PDA}(t) = \frac{3R_0^6}{2\tau_D}\frac{\kappa(t)^2}{R(t)^6} \quad \text{(S9)}$$

To account for orientational dynamics of the dyes, we then adopt the following expression for the transfer efficiency, which allows to incorporate static and dynamic disorder by separating slow and fast fluctuations in instantaneous transfer rates:[2]

$$E_{theo} = \left\langle\frac{1}{1+\frac{1}{\tau_D\langle k_{theo}(t)\rangle_{fast}}}\right\rangle_{slow} \quad \text{(S10)}$$

Where $\langle\ldots\rangle_{fast}$ is an average over fluctuations that are fast compared to the *D* excited state lifetime, whereas $\langle\ldots\rangle_{fast}$ subsequently averages over static disorder. This procedure was shown to provide efficiencies in excellent agreement with direct Monte Carlo simulations of the efficiencies along MD trajectories.[2] In addition, fluorescence lifetime distributions and decays were derived from the transfer rates using the following expression.

$$\tau_f = \frac{1}{k_D+\langle k_{theo}(t)\rangle_{fast}} \quad \text{(S11)}$$

$$I = \left\langle e^{-\left(k_D+\langle k_{theo}(t)\rangle_{fast}\right)t}\right\rangle_{slow} \quad \text{(S12)}$$

1.2 TrESP-MMPol model

The electronic coupling for singlet-singlet energy transfer involving bright states is dominated by coulombic and environment-mediated contributions:

$$V = V_{Coul} + V_{env} \tag{S13}$$

These contributions can be obtained using linear response time-dependent density functional theory (TD-DFT) in a polarizable quantum/molecular mechanical (QM/MMPol) framework, where the environment is described by atomic charges and isotropic polarizabilities:[1,3]

$$V_{Coul} = \int d\boldsymbol{r} \int d\boldsymbol{r}' \rho_D^{T*}(\boldsymbol{r}') \frac{1}{|\boldsymbol{r}-\boldsymbol{r}'|} \rho_A^T(\boldsymbol{r}) \tag{S14}$$

$$V_{env} = -\sum_l \int d\boldsymbol{r}' \rho_D^{T*}(\boldsymbol{r}') \frac{(\boldsymbol{r}'-\boldsymbol{r}_l)}{|\boldsymbol{r}'-\boldsymbol{r}_l|^3} \cdot \boldsymbol{\mu}_l^{MMPol}(\rho_A^T) \tag{S15}$$

where short-range contributions are neglected and the transition densities $\rho_{A/D}^T$ for the *D* and *A* molecules describe the diagonal part of the one-particle density matrix constructed from the ground and excited-state wave functions.

One can then define an effective dielectric constant for the environment as

$$s = \frac{1}{\varepsilon_{eff}} = \frac{V_{Coul}+V_{env}}{V_{Coul}} \tag{S16}$$

Using this expression, the total coupling can be expressed as $V = sV_{Coul}$, providing a direct link to the coulombic term and the screening factor in Förster coupling expression Eq. (S2), $V \approx sV_{PDA} = 1/\varepsilon_{opt} \cdot V_{PDA}$. Thus, the PDA approximation simplifies the description of the transition densities using transition dipole moments. The limits of this model at close separations comparable of the dimensions of the dyes are well-known.[4,5] A more practical simplification, however, relies on approximating the transition densities as a distributed transition monopole distribution,[6–8] i.e. a set of atomic transition charges like those widely used in classical force fields. Here, we adopt a TrESP-MMPol model,[9] in which charges are fitted to reproduce the electrostatic potential generated by QM-derived transition densities,[10] which leads to the following expressions:

$$V_{Coul,TrESP} = \sum_{i,j} \frac{q_{D,i}^T q_{A,j}^T}{|\boldsymbol{r}_i - \boldsymbol{r}_j|} \quad \text{(S17)}$$

$$V_{env,TrESP} = -\sum_{i,l} \frac{q_{D,i}^T (\boldsymbol{r}_i - \boldsymbol{r}_l) \cdot \boldsymbol{\mu}_l^{MMPol}(\{q_A^T\})}{|\boldsymbol{r}_i - \boldsymbol{r}_l|^3} \quad \text{(S18)}$$

where $q_{D,i}^T$ and $q_{A,j}^T$ indicate transition charges on the D/A atoms *i* and *j*, respectively. These expressions allow us to compute FRET couplings with full account of the atomistic heterogeneous environment of the dyes for the extensive sets of frames explored in MD simulations.

1.3 MD simulations

Initial systems were prepared starting from the human *holo* structure of CaM solved at 1.7 Å resolution (PDB ID 1CLL).[11] We considered CaM with mutations T34C and T110C labelled at these positions with donor/acceptor dyes Alexa Fluor 488 C5 maleimide (AF488) and Texas Red C2 maleimide (TRC2). In particular, we prepared two systems, *holo* CaM-AF488-TRC2 and CaM-TRC2-AF488 systems, with donor/acceptor dyes placed on 34/110 or 110/34 positions, in order to reproduce the experimental mixture. Missing residues and the C- and N-terminal ends were added manually, and all amino acids were considered in their standard protonation state as predicted by PROPKA3 calculations.[12] Simulations were based on the Amber ff14SB protein force field,[13] the TIP3P water model,[14] the Joung-Cheatham parameters for monovalent ions[15] and the Li-Merz parameters for Ca^{2+}.[16] AF488 and TRC2 dyes were described using the Amber GAFF2 force field, with RESP charges derived at the HF/6-31G(d) level of theory on geometries obtained using CAM-B3LYP/6-31G(d) including Grimme D3 dispersion correction.[17] All systems were solvated in a 0.1 M KCl aqueous solution octahedral box, minimized and then thermalized from 0 K to 300 K during 250 ps NVT simulations followed by 250 ps equilibration in the NPT ensemble. Then, NVT production runs were extended for 5 μs. This procedure was performed for a total of 3 × 5 μs replicas for each system CaM-AF488-TRC2 and CaM-TRC2-AF488. All simulations were performed using the Amber20 software[18] using periodic boundary conditions, the SHAKE algorithm to restrain bonds involving hydrogen, the particle-mesh Ewald approach to account for long-range electrostatics, a nonbonded cutoff equal to 10 Å, and the Hydrogen Mass Repartitioning scheme, [19] which allowed an integration time step of 4 fs. RMSD and R_g analysis were performed on trajectories with frames saved every 20 ps.

1.4 Electronic coupling calculations

In electronic coupling calculations, the MMPol environment was described using the Amber pol12 AL polarizable force field,[20,21] whereas the dyes were described either using TD-DFT (QM/MMPol) or adopting a distributed model of atom-centered transition charges (TrESP/MMPol). We explored the performance of different DFT functionals to describe the couplings between the relevant π-π* excited states of the dyes, including M06, B3LYP, CAM-B3LYP, PBE, PBE0, M06-2X. We selected CAM-B3LYP, which led to a simpler identification of the state of interest among different structures, although our results indicated that electronic couplings are rather robust regarding the choice of QM method and basis set, in line with previous studies.[1,22] After test calculations, we also defined the boundaries between MMPol and the QM regions in the bond between the linker and the phenyl ring bound to the choromophoric system of the dyes using the link atom scheme.[23] Atomic charges for water were taken from previous work,[24] whereas polarization-consistent ESP charges for AF488 and TRC2 dyes were derived using the Polchat tool at the B3LYP/6-31G(d) level of theory.[25] For K^+ and Ca^{2+} cations not defined in the pol12 AL polarizable force field,[20,21] atomic polarizabilities were computed at the CCSD(T)/6-311++G(d,p) level of theory. On the other hand, TrESP charges corresponding to the transition between the ground and excited state of the dyes were derived from TD-CAM-B3LYP/6-31G(d) calculations in IEFPCM water solvent on the optimized geometries described in the previous section. The electrostatic potential (ESP) from the transition densities was computed using Gaussian at points selected according to the Merz-Singh-Kollman scheme using 10 van der Waals layers and a density of 10 points per unit area, and were fitted to a set of atomic charges using the TraDA tool.[26] QM/MMPol calculations were performed using a locally modified development version of the Gaussian package,[27] while TrESP-MMPol calculations were run using the Trespcoup software.[28]

The TrESP/MMPol model was initially benchmarked with full QM/MMPol calculations.[3] Because screening effects markedly depend on the choice of MMPol cutoff radius, which defines the spatial extent of the polarizable MM region,[29] we first explored this dependence for 9 structures extracted from the trajectory of CaM-AF488-TRC2 spanning a range of interdye distances between 15-70 Å). In these calculations, explicit polarization was limited to residues within the MMPol cutoff radius from the QM region, whereas remaining residues up to a 35 Å were described through the additive Amber force field. As shown in Figures S1, acceptable

errors were obtained using a value ~15-20 Å for the MMPol cutoff radius, thus we fixed this value to 20 Å.

We then benchmarked TrESP/MMPol couplings with QM/MMPol TD-CAM-B3LYP/6-31G(d) couplings for an extended set of 100 structures extracted from the MD trajectories. TrESP/MMPol couplings were computed adopting a MMPol cutoff radius equal to 10, 15 or 20 Å. The results, shown in Figure S2, indicate that a value of 15 Å provides accurate results while keeping computational cost low, so this value was adopted for all further TrESP/MMPol calculations performed every 20 ps on the 3 × 5 μs MD trajectories obtained for each system: CaM-AF488-TRC2 and CaM-TRC2-AF488.

FRET rates defined in Eq. S8 and S9 were obtained using a refractive index $n^2 = 2$,[30] a critical Förster radius $R_0 = 54$ Å[31] and a fluorescence lifetime for AF488 $\tau_D = 4$ ns.[32] Transition dipole moments for the AF488 donor and TRC2 acceptor equal to $\mu_D = 7.56\ D$ and $\mu_A = 10.19\ D$ were extracted from the TD-DFT calculations used to parametrized the TrESP charges. The center-to-center distance between dyes $R(t)$ and the $\kappa(t)$ orientation factors were computed from the structures sampled along the MD trajectories. Finally, to dissect the impact of Förster approximations, we defined four coupling models (PDA, PDA-MMPol, TrESP, TrESP-MMPol) using the general expression $V = s \cdot V_{Coul}$, which combine a Coulomb term computed using the TrESP or the PDA approximation with a screening factor given by Förster $1/n^2$ value or derived using TrESP/MMpol calculations using Eq. S16-S18.

Table S1. Structural and FRET properties averaged over MD trajectories for *holo* CaM-AF488-TRC2 and CaM-TRC2-AF488 systems.[a]

	$\langle R \rangle$	$\langle \kappa^2 \rangle$	$\langle s \rangle^b$	$\langle V_{PDA}^2 \rangle$	$\langle V^2 \rangle^b$	$\langle k_{theo} \rangle^b$	$\langle \tau_D \rangle^b$	$\langle E_{theo} \rangle^b$
TRC2-AF488	41.0	0.56	0.71	3145	1487	368	0.78	0.80
AF488- TRC2	41.6	0.67	0.69	270	514	127	0.92	0.76
Total	41.3	0.62	0.70	1708	1001	247	0.85	0.78

[a]Distances R in Å, squared electronic couplings V_{PDA}^2 and V^2 in cm^{-2}, rates k_{theo} in ns^{-1} and excited state lifetimes τ_D in ns. [b]Properties derived from TrESP-MMPol electronic coupling calculations.

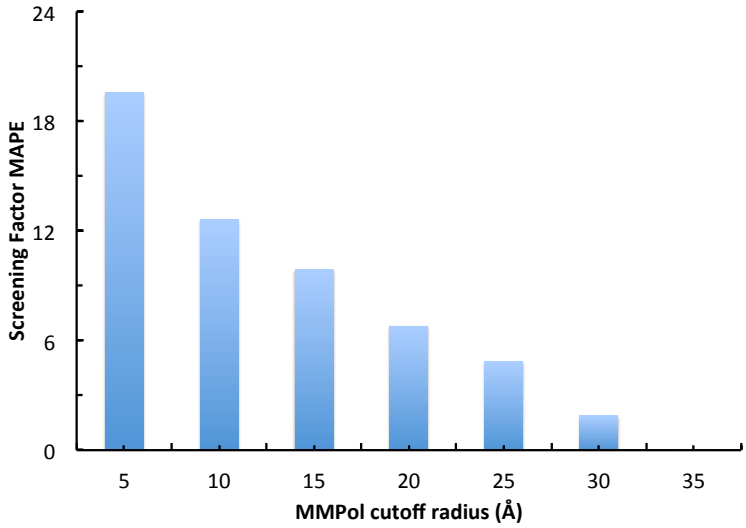

Figure S1. Mean absolute percentage error (MAPE) in screening factors computed using QM/MMPol for 9 selected structures of CaM-AF488-TRC2 using different values of MMPol cutoff radius.

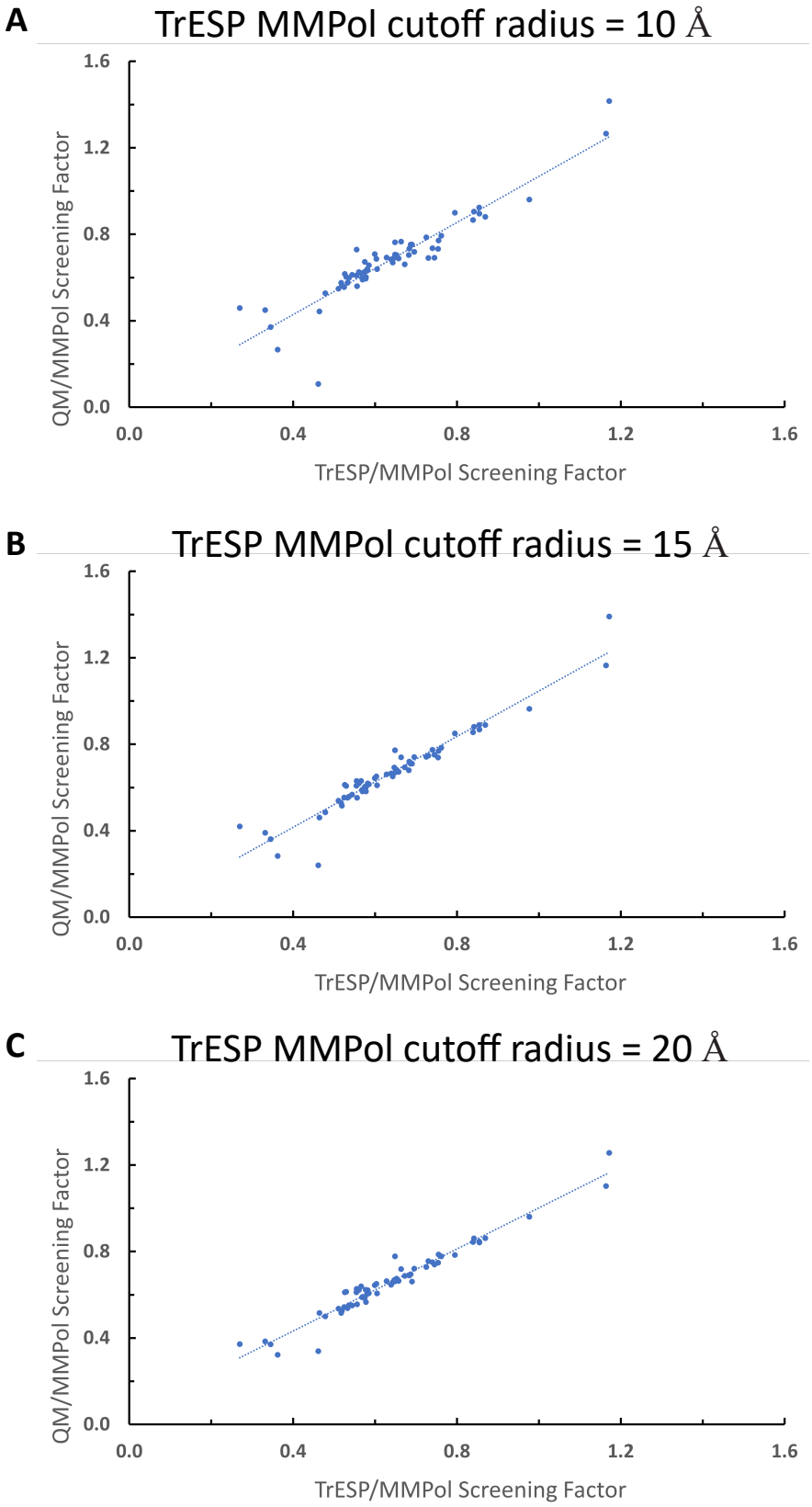

Figure S2. Comparison between QM/MMPol screening factors, obtained using a fixed 20 Å MMPol cutoff radius, with TrESP/MMPol values obtained for different values of the cutoff.

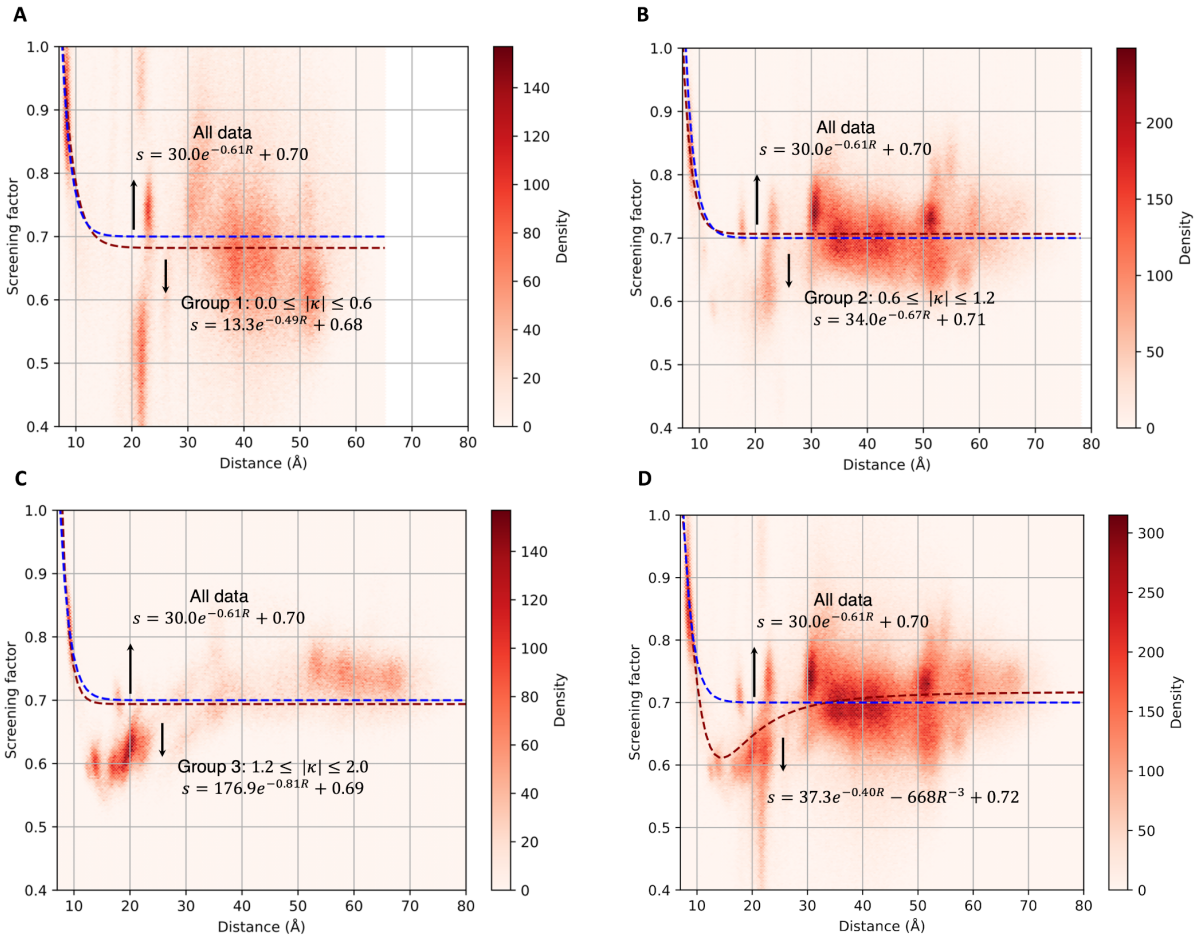

Figure S3. Density distribution of screening factors as a function of D/A separation derived from TrESP/MMPol electronic couplings computed for *holo* CaM-AF488-TRC2 and CaM-TRC2-AF488 systems along MD trajectories. Overall results are fitted to the empirical formula $s = 30.0e^{-0.61R} + 0.70$ and compared to analogous expressions fitted to subsets of the data based on κ dipole orientation factor: **A** Group 1 ($0.0 \leq \kappa \leq 0.6$); **B** Group 2: $0.6 \leq \kappa \leq 1.2$ and **C** Group 3: $1.2 \leq \kappa \leq 2.0$. **D** Comparison of the exponential empirical function with the analogous expression with an additional R^{-3} term to account for the minimum at separations ~15 Å.

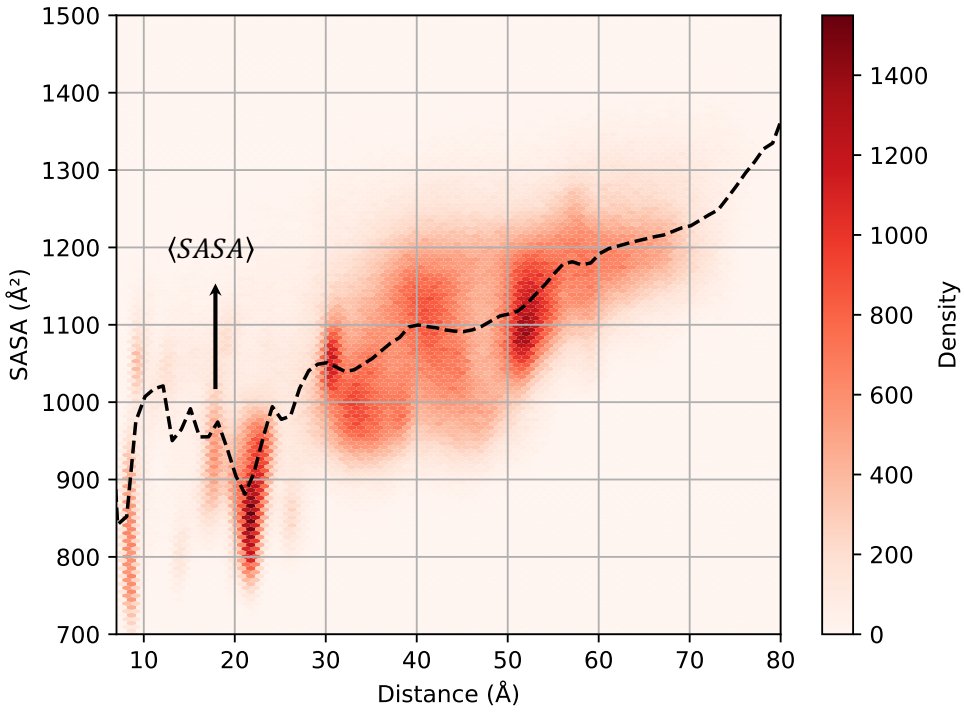

Figure S4. Contribution of the AF488 and TRC2 dyes to the total solvent-accessible surface area (SASA) of the *holo* CaM-AF488-TRC2 and CaM-TRC2-AF488 systems computed along MD trajectories. Surface area computed using the LCPO algorithm of Weiser et al.[33]

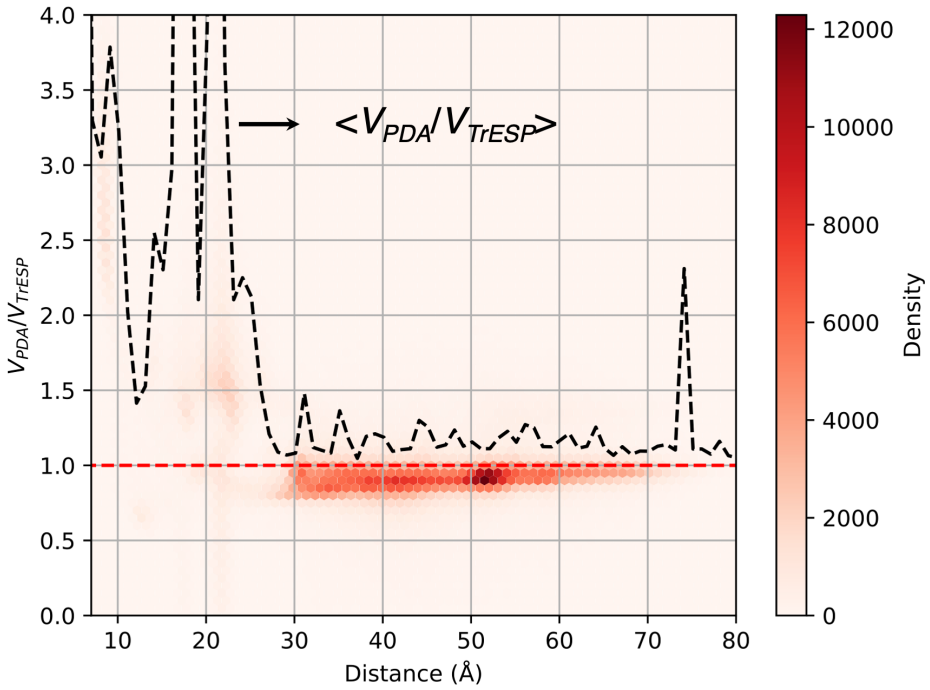

Figure S5. Ratio between PDA and TrESP coulombic coupling contributions (average values over distance bins indicated by black dashed curve).

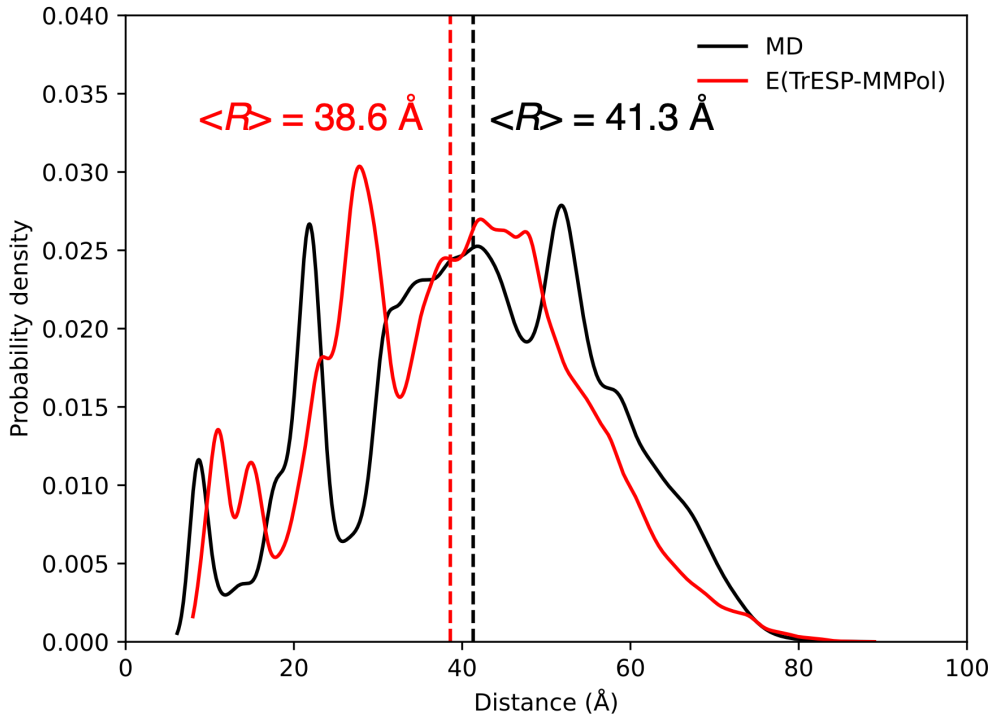

Figure S6. Distribution of donor-acceptor distances directly measured along MD trajectories or estimated using Eq. 3 from TrESP-MMPol FRET efficiencies.

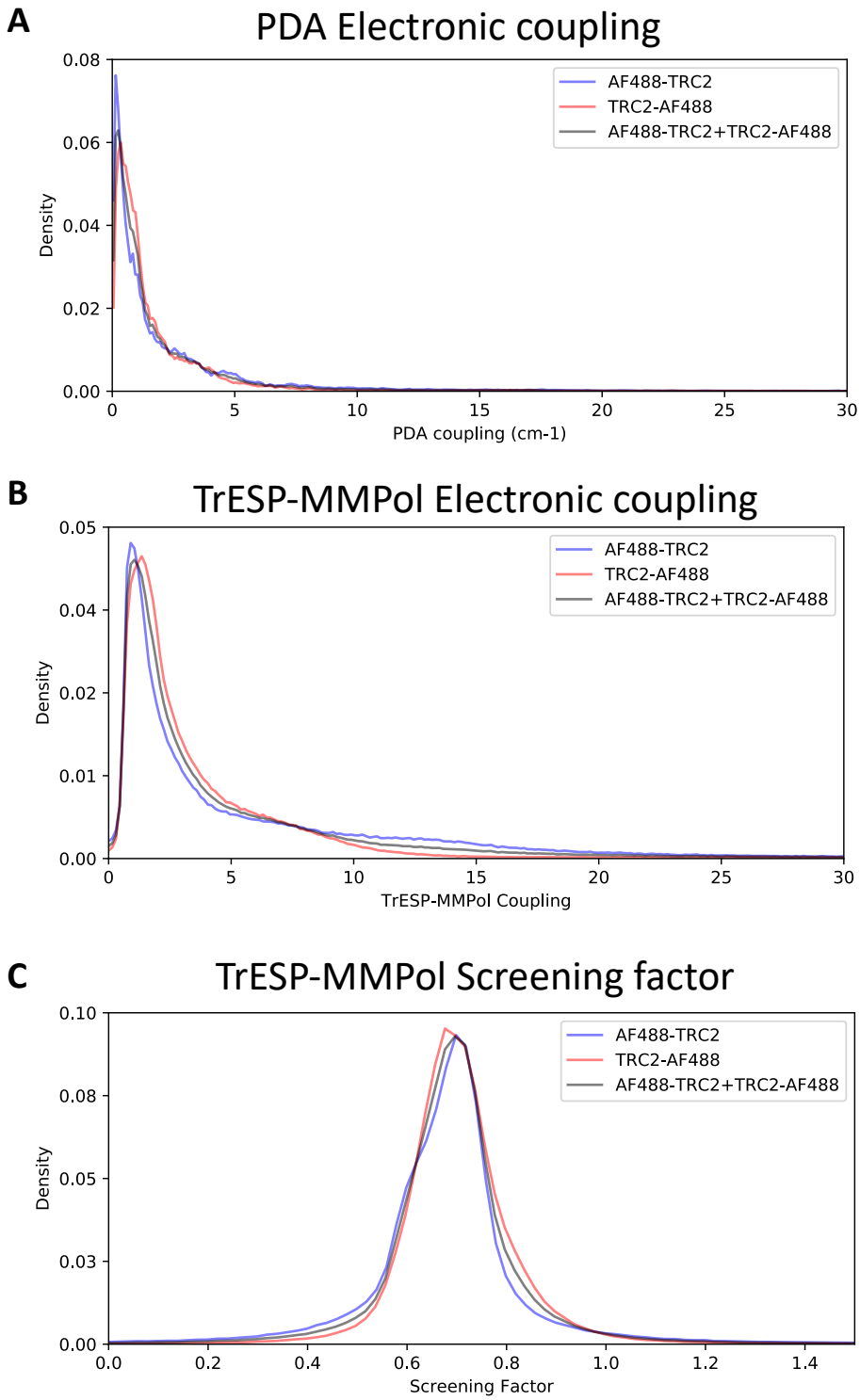

Figure S7. Electronic couplings and screening factors computed along MD trajectories for *holo* CaM-AF488-TRC2 and CaM-TRC2-AF488 systems.

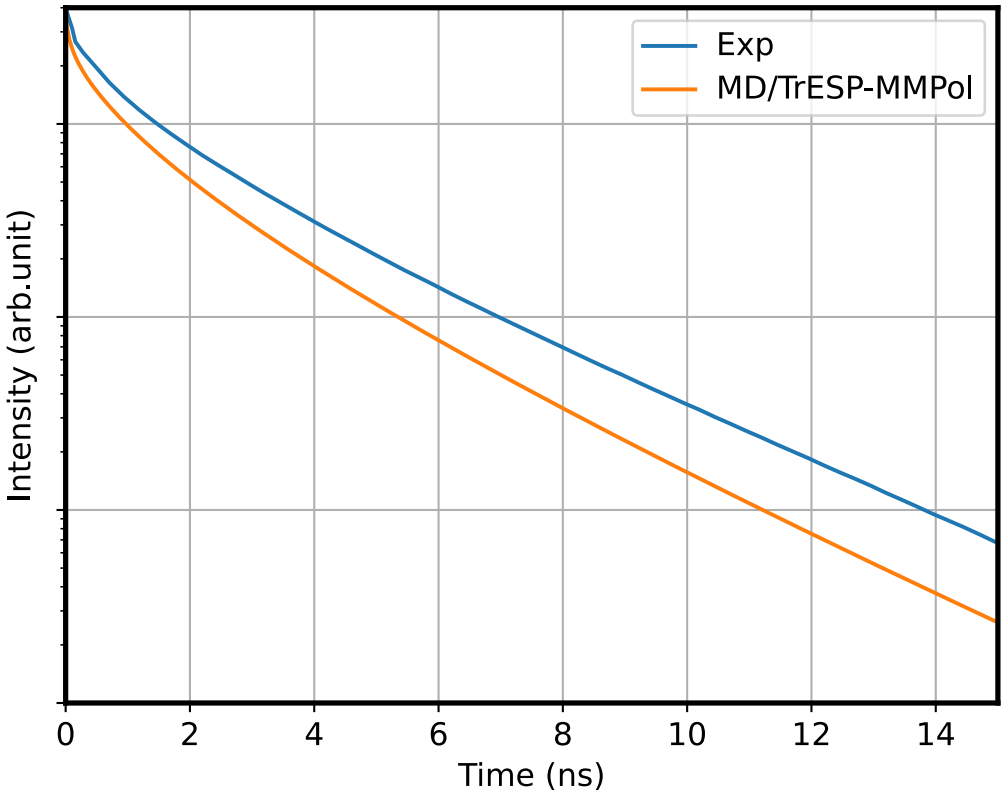

Figure S8. Fluorescence decay from MD/TrESP-MMPol data calculated for the two CaM systems compared to experiment.[31]

REFERENCES

1 L. Cupellini, M. Corbella, B. Mennucci and C. Curutchet, *Wiley Interdiscip Rev Comput Mol Sci*, 2019, **9**, e1392.

2 E. Sobakinskaya, M. Schmidt am Busch and T. Renger, *J Phys Chem B*, 2018, **122**, 54–67.

3 C. Curutchet, A. Munoz-Losa, S. Monti, J. Kongsted, G. D. Scholes and B. Mennucci, *J. Chem. Theory Comput.*, 2009, **5**, 1838–1848.

4 C. Curutchet and B. Mennucci, *Chem Rev*, 2017, **117**, 294–343.

5 A. Muñoz-Losa, C. Curutchet, B. P. Krueger, L. R. Hartsell and B. Mennucci, *Biophys. J.*, 2009, **96**, 4779–4788.

6 K. A. Kistler, F. C. Spano and S. Matsika, *J Phys Chem B*, 2013, **117**, 2032–2044.

7 J. C. Chang, *J Chem Phys*, 1977, **67**, 3901.

8 D. Beljonne, G. Pourtois, C. Silva, E. Hennebicq, L. M. Herz, R. H. Friend, G. D. Scholes, S. Setayesh, K. Mullen, J. L. Bredas, K. Müllen and J. L. Brédas, *Proc Natl Acad Sci U S A*, 2002, **99**, 10982–10987.

9 E. Cignoni, L. Cupellini and B. Mennucci, *Journal of Physics: Condensed Matter*, 2022, **34**, 304004.

10 M. E. Madjet, A. Abdurahman and T. Renger, *J Phys Chem B*, 2006, **110**, 17268–17281.

11 R. Chattopadhyaya, W. E. Meador, A. R. Means and F. A. Quiocho, *J Mol Biol*, 1992, **228**, 1177–1192.

12 M. H. M. Olsson, C. R. Søndergaard, M. Rostkowski and J. H. Jensen, *J Chem Theory Comput*, 2011, **7**, 525–537.

13 J. A. Maier, C. Martinez, K. Kasavajhala, L. Wickstrom, K. E. Hauser and C. Simmerling, *J Chem Theory Comput*, 2015, **11**, 3696–3713.

14 W. L. Jorgensen, J. Chandrasekhar, J. D. Madura, R. W. Impey and M. L. Klein, *J Chem Phys*, 1983, **79**, 926–935.

15 I. S. Joung and T. E. Cheatham, *J. Phys. Chem. B*, 2008, **112**, 9020–9041.

16 P. Li, B. P. Roberts, D. K. Chakravorty and K. M. Merz, *J Chem Theory Comput*, 2013, **9**, 2733–2748.

17 S. Grimme, J. Antony, S. Ehrlich and H. Krieg, *J Chem Phys*, 2010, **132**, 154104.

18 D. A. Case, K. Belfon, I. Y. Ben-Shalom, S. R. Brozell, D. S. Cerutti, T. E. Cheatham III, V. W. D. Cruzeiro, T. A. Darden, R. E. Duke, G. Giambasu, M. K. Gilson, H. Gohlke, A. W. Goetz, R. Harris, S. Izadi, S. A. Izmailov, K. Kasavajhala, A. Kovalenko, R. Krasny, T. Kurtzman, T. S. Lee, S. LeGrand, P. Li, C. Lin, J. Liu, T. Luchko, R. Luo, V. Man, K. M. Merz, Y. Miao, O. Mikhailovskii, G.

Monard, H. Nguyen, A. Onufriev, F. Pan, S. Pantano, R. Qi, D. R. Roe, A. Roitberg, C. Sagui, S. Schott-Verdugo, J. Shen, C. L. Simmerling, N. R. Skrynnikov, J. Smith, J. Swails, R. C. Walker, J. Wang, L. Wilson, R. M. Wolf, X. Wu, Y. Xiong, Y. Xue, M. York and P. A. Kollman, AMBER 2020, University of California, San Francisco 2020.

19 C. W. Hopkins, S. Le Grand, R. C. Walker and A. E. Roitberg, *J Chem Theory Comput*, 2015, **11**, 1864–1874.

20 J. Wang, P. Cieplak, J. Li, T. Hou, R. Luo and Y. Duan, *J. Phys. Chem. B*, 2011, **115**, 3091–3099.

21 J. Wang, P. Cieplak, J. Li, J. Wang, Q. Cai, M. Hsieh, H. Lei, R. Luo and Y. Duan, *J. Phys. Chem. B*, 2011, **115**, 3100–3111.

22 A. Muñoz-Losa, C. Curutchet, I. Fdez. Galván and B. Mennucci, *J Chem Phys*, 2008, **129**, 034104.

23 H. M. Senn and W. Thiel, *Angew. Chem. Int. Ed.*, 2009, **48**, 1198–1229.

24 M. Corbella, L. Cupellini, F. Lipparini, G. D. Scholes and C. Curutchet, *ChemPhotoChem*, 2019, **3**, 945–956.

25 S. Caprasecca, C. Curutchet, B. Mennucci, PolChat: A polarisation-consistent charge fitting tool, ver. 4.1.2, Molecolab Tools; University of Pisa. molecolab.dcci.unipi.it/tools. 2014–2018.

26 L. Cupellini, S. Jurinovich, B. Mennucci. TraDA - Transition Density Analyzer. Zenodo. https://doi.org/10.5281/zenodo.10966411 2024.

27 M. J. Frisch, G. W. Trucks, H. B. Schlegel, G. E. Scuseria, M. A. Robb, J. R. Cheeseman, G. Scalmani, V. Barone, B. Mennucci, G. A. Petersson, H. Nakatsuji, M. Caricato, X. Li, H. P. Hratchian, A. F. Izmaylov, J. Bloino, B. G. Janesko, F. Lipparini, G. Zheng, J. L. Sonnenberg, W. Liang, M. Hada, M. Ehara, K. Toyota, R. Fukuda, J. Hasegawa, M. Ishida, T. Nakajima, Y. Honda, O. Kitao, H. Nakai, T. Vreven, Jr. Montgomery J. A., J. E. Peralta, F. Ogliaro, M. Bearpark, J. J. Heyd, E. Brothers, K. N. Kudin, T. Staroverov, T. Keith, R. Kobayashi, K. Normand, J. Raghavachari, A. Rendell, J. C. Burant, S. S. Iyengar, J. Tomasi, M. Cossi, N. Rega, J. M. Millam, M. Klene, J. E. Knox, J. B. Cross, V. Bakken, C. Adamo, J. Jaramillo, R. Gomperts, R. E. Stratmann, O. Yazyev, A. J. Austin, R. Cammi, C. Pomelli, J. W. Ochterski, R. L. Martin, K. Morokuma, V. G. Zakrzewski, G. A. Voth, P. Salvador, J. J. Dannenberg, S. Dapprich, P. V. Parandekar, N. J. Mayhall, A. D. Daniels, O. Farkas, J. B. Foresman, J. V. Ortiz, J. Cioslowski and D. J. Fox. Gaussian development version, revision H.36. Wallingford CT: Gaussian, Inc. 2010.

28 L. Cupellini, F. Lipparini, E. Cignoni. trespcoup - Software to compute TrEsp couplings. Zenodo. https://doi.org/10.5281/zenodo.10966391 2024.

29 C. Curutchet, J. Kongsted, A. Muñoz-Losa, H. Hossein-Nejad, G. D. Scholes and B. Mennucci, *J. Am. Chem. Soc.*, 2011, **133**, 3078–3084.

30 X. J. Jordanides, M. J. Lang, X. Song and G. R. Fleming, *J. Phys. Chem. B*, 1999, **103**, 7995–8005.

31 M. S. DeVore, A. Braimah, D. R. Benson and C. K. Johnson, *J Phys Chem B*, 2016, **120**, 4357–4364.

32 B. D. Slaughter, M. W. Allen, J. R. Unruh, R. J. Bieber Urbauer and C. K. Johnson, *J. Phys. Chem. B*, 2004, **108**, 10388–10397.

33 J. Weiser, P. S. Shenkin and W. C. Still, *J Comput Chem*, 1999, **20**, 217–230.